Frying doughnuts: What can the reprocessing of X-rays to IR tell us about the AGN environment?

B. McKernan[1,2]⋆, K.E.S. Ford[1,2], N. Chang[1] & C.S. Reynolds[3]

[1] *Department of Science, Borough of Manhattan Community College, City University of New York, New York, NY 10007*
[2] *Department of Astrophysics & Hayden Planetarium, American Museum of Natural History, New York, NY 10024*
[3] *Department of Astronomy, University of Maryland College Park, College Park, MD 21242*

ABSTRACT

Active galactic nuclei (AGN) produce vast amounts of high energy radiation deep in their central engines. X-rays either escape the AGN or are absorbed and re-emitted mostly as IR. By studying the dispersion in the ratio of observed mid-IR luminosity to observed 2-10keV X-ray luminosity ($R_{ir/x}$) in AGN we can investigate the reprocessing material (possibly a torus or donut of dust) in the AGN central engine, independent of model assumptions.

We studied the ratio of observed mid-IR and 2-10keV X-ray luminosities in a heterogeneous sample of 245 AGN from the literature. We found that when we removed AGN with prominent jets, $\sim 90\%$ of Type I AGN lay within a very tight dispersion in luminosity ratio ($1 < R_{ir/x} < 30$). This implies that the AGN central engine is extremely uniform and models of the physical AGN environment (e.g. cloud cover, turbulent disk, opening angle of absorbing structures such as dusty tori) must span a very narrow range of parameters. We also found that the far-IR(100μm) to mid-IR (12μm) observed luminosity ratio is an effective descriminator between heavily obscured AGN and relatively unobscured AGN.

Key words: galaxies: active – galaxies: individual – galaxies: Seyfert – techniques: spectroscopic – X-rays: line – emission: accretion – disks :galaxies

1 INTRODUCTION

Active galactic nuclei (AGN) are powered by the accretion of matter onto a supermassive ($\sim 10^{[6,9]} M_\odot$) black hole. X-ray continuum emission from AGN (without jets) is believed to originate in the innermost regions of the AGN whereas IR continuum emission is believed to originate in dusty, cooler outer regions. The IR emission from AGN is due to a combination of reprocessed higher energy emission as well as thermal emission from star formation. Much if not most of the IR due to reprocessing comes from energy dumped in cool dusty material (mostly out of the observers' X-ray sightline) by photons with the most energy (X-rays). A comparison of the dispersion in the IR to X-ray luminosity ratios ($R_{ir/x}$) of a wide variety of AGN should therefore allow us to constrain the range of physical properties and geometry of the X-ray reprocessing material in AGN, independent of model assumptions.

The standard model of AGN explains the wide range of properties of observed AGN in terms of viewing angle,

since the equatorial flared disk expected at the heart of AGN breaks spherical symmetry (Antonucci 1993). However, partially or heavily obscured AGN need not be edge on, since obscuring material only needs to block the observer's sightline (see e.g. McKernan & Yaqoob 1998; Risaliti, Elvis & Nicastro 2002; Miller, Turner & Reeves 2008). Radiation reprocessing occurs in cool (possibly obscuring) material distributed around the AGN. Independent of assumptions about the distribution of cool material, the *dispersion* in $R_{ir/x}$ can constrain the range of possible geometries and physical conditions of the obscuring, reprocessing material around the central engine. The dispersion of $R_{ir/x}$ among AGN also provides information about depopulation or selection effects (bias), if there are values of $R_{ir/x}$ that are not favoured by AGN. Genuine depopulation in $R_{ir/x}$ space would yield model-independent information on allowed configurations of the AGN central engine.

The IR and X-ray emission in AGN have been compared in many previous studies (Boller et al. 1992; Green, Anderson & Ward 1992; Lutz et al. 2001; Krabbe et al. 2001; Horst et al. 2007; Mushotzky et al. 2008). Most recently Horst et al. (2007) reveal a strong

---

⋆ E-mail:bmckernan at amnh.org (BMcK)

correlation between modelled intrinsic 2-10keV X-ray luminosity and near-IR nuclear luminosity, suggestive of a 'leaky' torus of dust. Mushotzky et al. (2008) find a strong correlation between mid-IR luminosity and the very hard X-ray (14-195keV) observed luminosity, which is unaffected by absorption and indicates that the same phenomenon underlies all AGN. However, as yet there have been no comparisons of the observed hard 2-10keV X-ray luminosity with the IRAS band (12-100μm) IR luminosities. The 2-10keV X-rays are energetic enough to emerge with relatively mild attentuation through Compton-thin obscurers with absorption becoming more substantial above $N_H \sim 10^{22} \mathrm{cm}^{-2}$. Attenuated X-rays will mostly re-emerge as IR emission. Therefore, in tandem with IRAS band IR emission, 2-10keV X-rays are a good probe of absorption and subsequent reprocessing in the obscuring material around AGN. In this paper, for the first time, we studied the ratio of observed 2-10keV X-ray emission to IRAS band (12-100μm) IR emission for a large, heterogeneous sample of AGN. By studying dispersions in the luminosity ratio $R_{ir/x}$ of our sample, we hope to obtain information about the *dispersion* of physical properties of the AGN environment, independent of model assumptions.

In section 2 we briefly discuss X-ray and IR luminosity of AGN, including previous studies which compared emission in the two bands, and in section 3 we discuss our sample of AGN and associated caveats. In section 4, we explore the distribution of our sample of AGN in $R_{ir/x}$ parameter space and we use AGN classification and well-known AGN to constrain the dispersion of AGN in $R_{ir/x}$. In section 5 we attempt to rule out selection bias as an explanation of the dispersion of AGN in $R_{ir/x}$ space. In section 6 we discuss our results and establish model-independent constraints on the reprocessing material around AGN. Section 7 outlines our conclusions.

2   COMPARING X-RAY AND IR EMISSION FROM AGN

Most AGN are characterized by an SED that extends at least from the IR band to the hard X-ray band, cutting off at ∼50-300 keV (Perola et al. 2002). The broadband SED of these AGN can therefore always be characterized in a naive way by the slope from the IR band to the X-ray band. The IR band emission in most Seyfert AGN generally peaks in the IRAS band (12-100μm). The X-ray flux from Seyferts is typically strongly absorbed at energies <2keV (even at relatively low columns of $N_H \sim 10^{21} \mathrm{cm}^{-2}$) and fluxes at > 10keV are often too low to be strongly constrained, so a widely accepted measure of X-ray emission from AGN is the observed 2-10keV flux. Absorption of 2-10keV X-rays becomes more substantial at columns $N_H >\sim 10^{22} \mathrm{cm}^{-2}$ and so 2-10keV X-rays are a useful probe of Compton-thin absorbers along the AGN sightline, as well as reprocessing in the AGN environment. By comparing the ratio of observed 2-10 keV X-ray to IRAS-band IR emission from AGN, we therefore have (1) an approximate measure of steepness over the entire SED in most AGN independent of cosmology and (2) sufficient data from AGN to build a statistically meaningful sample.

The observed 2-10 keV X-ray flux from an AGN may not be the *intrinsic* X-ray flux of the AGN. With sufficiently large absorbing columns the 2-10keV hard X-ray flux can be very strongly attenuated (particularly when the absorber is Compton-thick, i.e. $N_H > 1.5 \times 10^{24} \mathrm{cm}^{-2}$). However, it can been difficult to separate AGN with weak observed X-ray flux from those with genuinely weak intrinsic X-ray flux, without knowledge of the very hard X-ray flux (> 14 keV or so). With the advent of very hard X-ray detectors with sufficient effective area (e.g. SaX, Suzaku and the BAT detector on Swift), it has only recently become possible to observe AGN unbiased by X-ray absorption (see e.g. Tueller et al. (2008); Winter et al. (2008); Itoh et al. (2008); Mushotzky et al. (2008)). To illustrate the effect of absorption on the intrinsic X-ray luminosity, we shall compare the observed 2-10keV flux and the interpolated intrinsic 2-10keV flux inferred from very hard X-ray measurements for a number of well-known AGN (see §4 below). Throughout this paper, we shall refer to the *observed* 2-10keV luminosities of AGN, unless otherwise indicated.

Comparisons of X-ray and IR emission in large samples of AGN (and normal galaxies) find significant correlations. Green, Anderson & Ward (1992) found a correlations between 60μm IRAS luminosity and *Einstein* (0.5-4.5keV) soft X-ray luminosity. Boller et al. (1992) found correlations between IRAS far-IR luminosity (60μm) with the ROSAT 0.1-2.4keV soft X-ray luminosity. Both Green, Anderson & Ward (1992) and Boller et al. (1992) show a clear jump towards higher X-ray emission among broad line galaxies compared with narrow line galaxies, suggestive of increasing dominance of non-thermal emission. Correlations from such heterogeneous samples of AGN are important since they suggest that the same phenomenon underlies all AGN. More recently, Mushotzky et al. (2008) found a strong correlation ($L_{ir} \sim L_X^{1.25}$) between very hard X-ray luminosity (14-195keV) and mid-IR luminosity in a uniform sample of hard X-ray selected AGN. High angular resolution (nuclear) IR studies of AGN have also revealed a correlation between mid-IR luminosity (at 6μm, 10.5μm and 12.3μm respectively) and the modelled intrinsic hard X-ray luminosity (2-10keV) (Lutz et al. 2001; Krabbe et al. 2001; Horst et al. 2007). These studies found no significant difference in the average ratio of mid-IR luminosity to modelled intrinsic hard X-ray luminosity for AGN assumed to be face-on or edge-on, which they suggest implies the dusty torus is clumpy rather than continuous, since X-rays must be leaking out from the central regions through the torus (Lutz et al. 2001; Krabbe et al. 2001; Horst et al. 2007).

Distinguishing models of flared disks (likely to be continuous) from models of clumpy clouds of gas and dust is important. However, high resolution IR studies at present will: a) not resolve most AGN, so their statistics will be poor, b) generally include contamination from surrounding star-formation and narrow line regions anyway (Horst et al. 2007) and c) potentially lose information about the AGN-host galaxy and AGN-starburst connection. Such high resolution IR studies are also likely to introduce bias in favour of the nearest AGN and restrict the AGN sample size. By including all nuclear IR emission, we avoid assumptions about the central engine environment and we span the complete nuclear activity phenomenon. Furthermore, modelled intrinsic 2-10keV X-ray luminosities are a function of individual AGN spectral models which can vary dramatically in the lit-

Table 1. The studies from which our AGN sample was derived . Listed are study, year, total number of NED objects listed in each paper and number of unique AGN extracted by us from each study, which had both IRAS and 2-10keV X-ray flux measurements on NED. Many AGN were included in multiple studies. We did not include AGN with only upper limits in either the IRAS band or the 2-10keV band.

Study	Year	NED objects	Unique AGN
McKernan *et al.*	2007	15	15
Horst *et al.*	2007	29	10
Buchanan *et al.*	2006	55	14
Foschini *et al.*	2006	19	7
Shinozaki *et al.*	2006	51	15
Botte *et al.*	2005	10	4
Nagar, Falcke & Wilson	2005	250	36
Peterson *et al.*	2004	37	14
Lutz *et al.*	2004	71	12
Bian & Zhao	2003	41	7
Sanders *et al.*	2003	664	23
Schade, Boyle & Letawsky	2000	76	3
Grupe *et al.*	1999	76	4
Leighly	1999	23	5
Malizia *et al.*	1999	36	2
Turner *et al.*	1999	36	1
Bonatto *et al.*	1998	60	4
Gonzalez Delgado *et al.*	1997	55	3
Ho, Filippenko & Sargent	1997	91	13
Smith & Done	1996	36	2
Eracleous & Halpern	1994	108	7
Rush, Malkan & Spinoglio	1993	893	8
Boroson & Green	1992	86	31
Total		2802	245

erature often for the same dataset (see e.g. McKernan et al. (2007) and references therein). While estimates of observed 2-10keV X-ray luminosity can depend on the continuum model chosen (e.g. FeKα line, reflection continuum), ultimately the observed luminosity is determined simply by the statistical quality of the simplest model fit to the 2-10keV continuum. A statistically good fit to the data converges on the observed value of the 2-10keV luminosity, regardless of whether the underlying model is actually correct. However, inferring the actual intrinsic 2-10keV AGN luminosity from a model fit can be complicated. For example, some or most of the Fe K or reflected emission could originate in cold, neutral material outside the AGN central engine, or absorption by ionized gas (warm absorber or Fe edges) could be significant. Therefore, by using observed 2-10keV luminosities, we attempt to avoid assumptions about the AGN environment or individual model idiosyncrasies in estimating intrinsic X-ray luminosity. We can more accurately infer the *intrinsic* 2-10keV X-ray luminosity of many of the obscured AGN, by including information from very hard X-ray studies of AGN (e.g. Winter et al. (2008); Itoh et al. (2008)).

3 THE SAMPLE AND CAVEATS

In the spirit of previous surveys such as Green, Anderson & Ward (1992), Boller et al. (1992) and Veilleux & Osterbrock (1987), we assembled our sample from a broad range of AGN studies. Table 1 lists

the twenty three studies of a total of 2802 AGN from which we assembled 245 unique AGN with both IRAS data and 2-10keV data in NED [1]. Note that, as in previous such heterogeneous studies (Veilleux & Osterbrock 1987; Green, Anderson & Ward 1992; Boller et al. 1992), our sample is *not* intended to be complete. Rather, our intention was to draw upon a wide range of AGN studies, incorporating all types of AGN, in order to investigate if any trends in $R_{ir/x}$ emerge even with heterogeneous groups of data. The point of this study in effect, is to see where AGN lie in X-ray-IR luminosity ratio ($R_{ir/x}$) space and whether we can in principle deduce model-independent results from their dispersion. Clumps and scatters in an $R_{ir/x}$ plot can reveal valuable information on AGN depopulation and/or AGN selection effects. In future work, we will increase our sample size by expanding on the number of surveys in Table 1.

For estimates of the AGN X-ray and IR luminosity, we used NED flux measurements in each waveband and the NED luminosity distance estimate, which uses a WMAP cosmology (Spergel et al. 2003). Where there were multiple flux measurements, we used the mean flux value in that waveband. This will tend to bias our survey against including flaring periods or dramatically low states for individual AGN with multiple flux measurements. Generally, the error on the flux measurements listed by NED is $\sim 10-20\%$ in the X-ray band and $\sim 5-10\%$ in the IR band. However, AGN are by nature variable, sometimes extremely so. Of the 245 AGN in our study, 128 have multiple measurements of their 2-10keV X-ray flux. Of these 128 AGN, roughly half (56/128) vary by a factor of two or more, only $\sim$1/5th (24/128) vary by a factor of three or more and only $\sim$ 5% (6/128) vary by an order of magnitude or more. Therefore we estimate that the 2-10keV flux in $\sim$ 55% of the AGN in our sample varies by less than a factor of two and the flux in $\sim$ 80% of the AGN in our sample varies by less than a factor of three. In spite of several well known exceptions, relatively low X-ray variability among AGN in general is consistent with previous studies (see e.g. Markowitz & Edelson (2004)).

In the IRAS band, 93 of the 245 AGN in our sample have multiple measurements of their IRAS band flux. Of these 93 AGN, roughly one quarter (23/93) vary by a factor of two or more, only $\sim$ 10% (8/93) vary by a factor of three or more and only 1/93 varies by an order of magnitude or more. Therefore we estimate that in the IR band, the flux in $\sim$ 75% of the AGN in our sample varies by less than a factor of two and the flux in $\sim$ 90% of the AGN in our sample varies by less than a factor of three. If these numbers are relatively representative of the AGN in our sample, we estimate that the majority of AGN luminosity ratios in this study have errors of no more than a factor of $\sim$ 3 in both the X-ray and IR luminosities. Note that the X-ray and IR measurements used in this paper are almost always *not simultaneous*. However, in spite of intrinsic AGN variability and non-simultaneity of the data in most cases, it turns out that our simple approach reveals strong trends in the data (see §4 below).

Table 2 shows the breakdown of our AGN sample into NED classification and redshift. AGN classification and our

---

[1] http://nedwww.ipac.caltech.edu/

Table 2. Breakdown of our sample by redshift and object classification . AGN with NED classifications involving prominent jets (e.g. BL Lacs, BLRGs) have been excluded. The first number in columns 2 & 3 denotes the total number of Group 1 and Group 2 AGN in the corresponding z range (see §4 below for further discussion of Groups 1 & 2 and AGN classification). The numbers in brackets denote respectively: the number of Seyfert (Sy) AGN; the number of AGN classified as Seyfert plus (Sy+) something else (e.g. Starburst, H_{II} region, LINER, QSO); the number of non-Seyfert (NS) AGN.

Redshift Range	Group 1 (Sy,Sy+,NS)	Group 2 (Sy,Sy+,NS)
<0.005	9(3,6,0)	53(31,9,13)
0.005-0.049	56(50,6,0)	53(32,16,5)
0.05-0.099	16(12,4,0)	3(3,0,0)
0.1-0.199	18(14,4,0)	0
0.2-0.4	13(6,6,1)	0
Total	112	109

exclusion of AGN with prominent jets is discussed in more detail in §4 below. As far as AGN redshift is concerned, most ($\sim 85\%$) of the AGN in our sample are at low redshift ($z < 0.1$), so the 12μm IR flux and 2-10 keV band X-ray flux does not include large amounts of flux redshifted from higher energies. However, for a small fraction ($\sim 15\%$) of the higher luminosity AGN, the observed 12μm and 2-10 keV fluxes may correspond to fluxes in the AGN frame of $\sim 6-12$μm and $\sim 2-15$keV respectively. Generally in these AGN, high energy X-ray flux falls off faster than the near IR flux, so in the small fraction of very distant luminous AGN we expect $R_{ir/x}$ to be slightly larger *on average* than the nearby group 1 AGN (see also Fig. 11 and related discussion below).

In this paper, we discuss luminosity ratios. The IR flux is measured in Jy ($=3.0 \times 10^{-11}$ erg cm^{-2}s^{-1} at 100μm and 2.5×10^{-10} erg cm^{-2}s^{-1} at 12μm) and the X-ray flux is measured in units of 10^{-11} erg cm^{-2}s^{-1}. The luminosity (and flux) ratios described hereafter are unitless.

4   RELATIVE X-RAY AND INFRA-RED LUMINOSITIES OF AGN

In this section we will start by presenting our entire AGN sample in $R_{ir/x}$ space using observed 2-10keV X-ray and IRAS-band IR measurements. We shall then use AGN classifications to begin constraining the dispersions of different AGN types in $R_{ir/x}$. We shall also introduce well-known AGN 'typical' of their classification to aid interpretation of the AGN distribution. We shall then compare the distribution of AGN in $R_{ir/x}$ using far-IR (100μm) and mid-IR (12μm) observed luminosity.

Figure 1 shows the observed 2-10keV X-ray flux plotted against the 12μm mid-IR flux for 240/245 AGN in our sample (5 AGN had 12 μm upper limits only). Lines of constant flux ratio are plotted (Fir/Fx=1,10,100) to guide the eye. If we express the flux ratios from Figure 1 in terms of luminosity ratios, the *ratios* remain constant, but the AGN separate by a factor proportional to the distance squared.

Since jets will complicate our interpretation of the central engine, we excluded 20 AGN with NED classifications
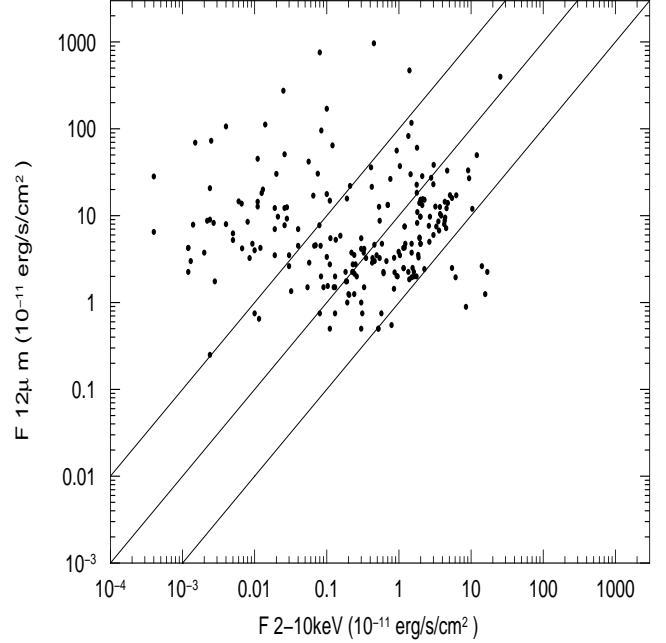

Figure 1. Mean 12μm IR flux (from IRAS/ISO) plotted against mean observed 2-10keV X-ray flux for 240/245 AGN in our sample (5 AGN had upper limits only at 12μm). Data (non-simultaneous) are taken from NED. Also plotted are lines of constant flux ratio (Fir/Fx=1,10,100).

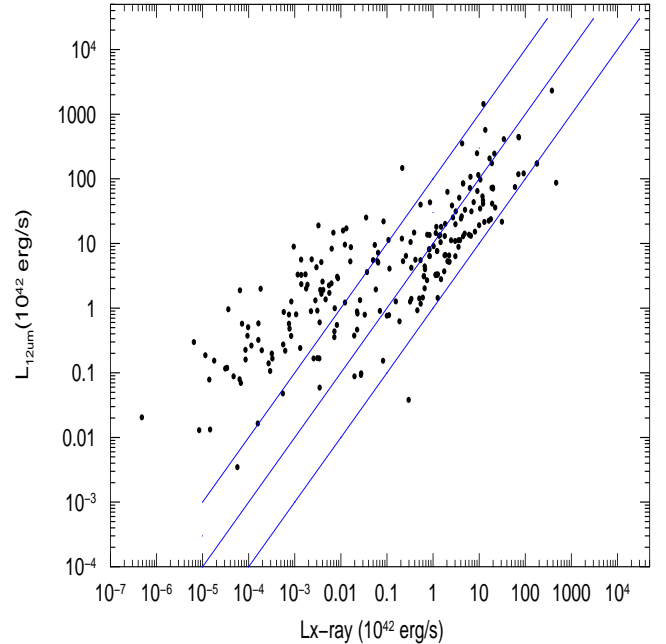**Figure 2.** Mean 12μm IR luminosity (from IRAS) plotted against mean 2-10keV X-ray luminosity for 215/245 AGN in our sample with NED classifications that do not include jets. Data (non-simultaneous) are taken from NED. Also plotted are lines of $R_{ir/x}$=1,10,100 to guide the eye.The three AGN with $R_{ir/x} < 1$ are, from bottom to top, Cen A, PG 1416-129 and PG 0026+129.

that include prominent jets (e.g. BL Lac, Blazar, LPQ, BLRG). Figure 2 shows the mean hard X-ray 2-10keV luminosity plotted against the mean mid-IR 12μm luminosity for 215/245 of the AGN in our sample. Lines of constant luminosity ratio ($R_{ir/x}$=1,10,100) are indicated to guide the eye. From Fig. 2, the more luminous AGN seem to emerge at $L_x, Lir \sim 10^{42-43}$ ergs s^{-1} and mostly lie in a band around $R_{ir/x} \sim [1, 30]$. Lower luminosity AGN appear to span a much wider range of observed luminosities, suggestive of both highly absorbed X-ray luminosity and/or a 'noisy' host galaxy background in IR or X-rays. The AGN in Fig. 2 span $R_{ir/x}$ space in a manner broadly similar to studies carried out using soft X-rays (Green, Anderson & Ward 1992; Boller et al. 1992).

Although we excluded AGN with prominent jets, the remaining AGN may well contain weak jets, but they are not prominent enough to effect AGN classification. AGN with prominent jets accounted for more than half the AGN with $L_x > 3 \times 10^{43}$ ergs s^{-1}, so if present and prominent, jets account for a significant proportion of X-ray luminosity. From Fig. 2, there are only 3/225 AGN with $R_{ir/x} < 1$, suggesting either that $R_{ir/x} < 1$ is atypical for AGN or that there is a bias against AGN with $R_{ir/x} < 1$ in our sample. It is noteworthy that the 3/215 AGN with $R_{ir/x} < 1$ in Fig. 2 have weak associated jets. They are, in order of increasing X-ray luminosity: Cen A, PG 1416-129 and PG 0026+129 respectively (Kraft et al. 2000; Porquet et al. 2007; Kukula et al. 1998). If this interpretation is correct, newly discovered AGN with $R_{ir/x} < 1$ should have associated jets.

At this point, it is useful to introduce AGN classification information (from NED) to aid further interpretation of the dispersion of $R_{ir/x}$ values among AGN. Broadly, we observe 'more active' and 'less active' AGN. Excluding AGN with jets, the 'more active' AGN population includes Seyfert 1s and some QSOs. The 'less active' population generally includes Seyfert 2s, LINERs, LLAGN, ULIRGs, some starburst-dominated AGN and some H$_{II}$ region-like galaxies (see e.g. the definition of 'emission line galaxies' for the sample in Veilleux & Osterbrock (1987)). Classifications are of course imperfect and so some AGN may overlap between these two groups, e.g. Seyfert 1.2-1.9 AGN, as well as cross-classified AGN (e.g. AGN classed both as Seyfert 1 and starburst or LINER & Seyfert 1.5). From Table 2 above, of the 221 AGN in our sample without prominent jets, 153/221 AGN are classified by NED purely as Seyferts (Sy 1,Sy1.2-1.9, Sy2), 49/221 AGN are classified as Sy+ or Seyfert plus something else (e.g. starburst, H$_{II}$ region, LINERs) and only 19/221 are non-Seyfert AGN. The 49/221 AGN classified as Sy+ highlight the difficulty of relying too heavily on AGN classifications, since the observed properties of many AGN cannot be forced into simple classifications. Such cross-classification also demonstrates the importance of an approach such as ours; namely a simple comparison of observables across a wide range of AGN activity.

We categorized the remaining 215/245 AGN in our sample based on their NED classification. Group 1 includes AGN classified by NED as Seyfert 1 and QSOs. Also included in group 1 are AGN which might overlap between Groups 1 and 2 (e.g. Seyfert 1.2-1.9 AGN and cross-classified AGN). Group 2 AGN includes AGN classified by NED as Seyfert 2, low luminosity AGN (LLAGN), LINERs, ULIRGs and star-
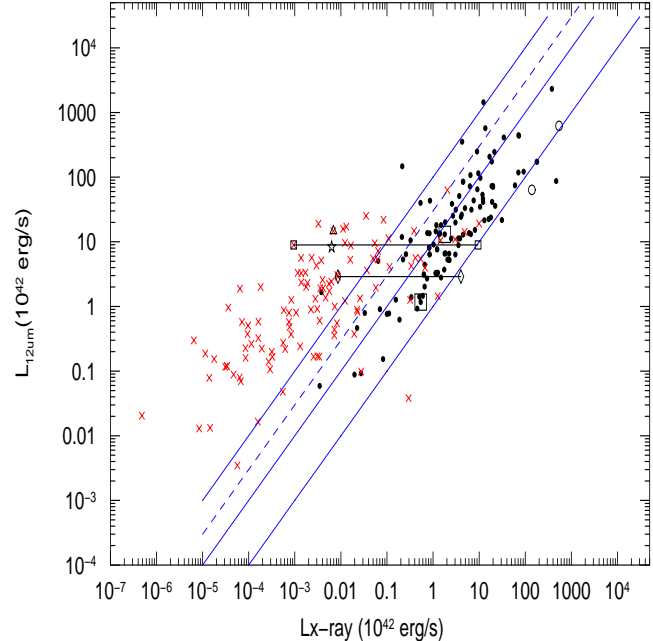

Figure 3. As Fig. 2 except we divided our AGN sample into the 'more active' Group 1 AGN (black circles) and 'less active' Group 2 AGN (red crosses) (see text for details). Dashed line indicates $R_{ir/x}$=30. Also highlighted are several well-known AGN to aid orientation: Open circles are 3c273 (upper) and PKS 2155-304 (lower), examples of a Blazar and BL Lac respectively (Note $R < 1$ in both cases). Giant open squares (with no lines) are centered on Akn 564 (upper) and MCG-6-30-15 (lower), examples of a narrow line Seyfert 1 (1.8) and Seyfert 1 (1.5) respectively. The open triangle is NGC 1068, a Seyfert 2 seen in reflection in X-rays and the open star is Arp 220, a starburst galaxy. Open squares with line correspond to the observed (left) & intrinsic (right) X-ray luminosities of NGC 4945 (Itoh et al. (2008)), a Compton-thick AGN seen in transmission. Open diamonds with line correspond to the observed (left) & intrinsic (right) X-ray luminosities of the Circinus galaxy (Matt et al. (1999)). Note that the intrinsic X-ray luminosities for NGC 4945 & Circinus were established from very hard X-ray measurements (independent of absorption).

burst dominated AGN. Table 2 shows that most of the AGN in our sample with these latter classifications are also classified as Seyfert AGN, again indicating the complexities of AGN classifications. Fig. 3 shows the two AGN populations highlighted with a dashed line indicating $R_{ir/x} = 30$. Also indicated are a few very well-known 'archetypal' AGN. We included two well-known AGN with jets, the Blazar 3C 273 and the BL Lac PKS 2155-304 (indicated by open circles). These two AGN have some of the smallest observed luminosity ratios ($R_{ir/x} \leqslant 1$) and are associated with jets close to their sightlines. The Seyfert 1 AGN (MCG-6-30-15 and Akn 564, indicated by giant squares) have mid-range values of $R_{ir/x}$ for Group 1 AGN. The starburst galaxy, Arp 220 (open star) has $R_{ir/x} \sim 1000$, as has the Seyfert 2 AGN NGC 1068 (open triangle). The open symbols connected by lines in Fig. 3 denote the luminosity ratios for the Compton thick AGN NGC 4945 (squares) and Circinus (diamonds) respectively, calculated using both the observed (left point) and *interpolated intrinsic* (right point) 2-10keV luminosity.

From Fig. 3, Group 1 AGN (black circles) are the more luminous AGN and have a remarkably narrow dispersion in luminosity ratio ($30 < R_{ir/x} < 1$) for most (97/107) Group 1 AGN. Of the ten Group 1 AGN with $R_{ir/x} > 30$, four are cross-classified (i.e. Seyfert 1 plus starburst) and four are heavily obscured Seyfert 1s ($N_H \sim 10^{23}\mathrm{cm}^{-2}$). So Group 1 AGN with $R_{ir/x} > 30$ could be accounted for either by the addition of IR luminosity from star formation or a drop in observed X-ray luminosity due to a change in partial-covering absorption (McKernan & Yaqoob 1998; Risaliti et al. 2002; Miller et al. 2008). So even with our simple approach, Fig. 3 indicates that $\sim 90\%$ of Group 1 AGN in our sample have $1 < R_{ir/x} < 30$. By contrast, Group 2 AGN (red crosses) generally have lower X-ray luminosities and have a wider dispersion in $R_{ir/x}$ than Group 1 AGN. In contrast to the Group 1 AGN, 97/109 group 2 AGN have $R_{ir/x} > 30$, with 83/109 group 2 AGN having $R_{ir/x} > 100$. Of the 12/109 Group 2 AGN with $1 < R < 30$ (i.e. overlapping with the main Group 1 population), we find that six have associated radio jets and two are Compton-thin Seyfert 2 AGN. From Table 2, 19/221 AGN in our sample are non-Seyferts, of which 10 are LINERs, 8 LINERs with H_{II} regions and 1 QSO. The LINERs lie in the bottom left hand corner of the Group 2 distribution ($L_{ir} < 0.5 \times 10^{42}$ erg/s, $L_x < 10^{39}$ erg/s) and the LINERs with H_{II} regions span a slightly larger range of the Group 2 distribution ($L_{ir} < 5 \times 10^{42}$ erg/s, $L_x < 10^{40}$ erg/s).

A key point from Fig. 3 is that the luminosity ratio for NGC 4945 and Circinus as calculated from the interpolated intrinsic 2-10keV luminosity (right point) lies in the main luminosity ratio band of Group 1 AGN. This is a nice demonstration of the fact that behind the Compton-thick obscuration of NGC 4945 and Circinus, lies the same phenomenon as in most Group 1 AGN. Without very hard X-ray measurements, it is very difficult to estimate intrinsic 2-10keV X-ray luminosities for most Group 2 AGN in our sample and certainly any such estimates would be highly model-dependent. Nevertheless, the examples of NGC 4945 and Circinus indicate that the *intrinsic* luminosity ratios for many Group 2 AGN may be similar to the Group 1 luminosity ratio range ($\sim 30 \leqslant R_{ir/x} \leqslant 1$). However, there are many model-dependent caveats in estimating the intrinsic X-ray luminosity of an AGN, so in §6 below we will take a different approach to Lutz et al. (2001); Krabbe et al. (2001); Horst et al. (2007) and attempt to derive constraints on AGN using *observed* luminosities.

Figure 4 shows the mean far-IR (100μm) luminosity of the AGN in our sample versus the mean 2-10keV observed X-ray luminosity. Note that several AGN had NED flux measurements at 12μm but only upper limits at 100μm and vice versa, so there is not a perfect one-to-one correspondence between all points on Fig. 4 and Fig. 3. Nevertheless, the dispersion in $R_{ir/x}$ for the Group 2 AGN in particular seems to be larger in Fig. 4 than in Fig. 3 and the various archetypal Group 2 AGN appear more separated in luminosity ratio. For example, the starburst galaxy Arp 220 (open star) is much more clearly distinguished from the classic Type 2 AGN NGC 1068 (open triangle) in Fig. 4 than in Fig 3. The non-Seyfert AGN, e.g. the LINERs and LINERs with H_{II} regions, are also highlighted. As we should expect from such low X-ray and IR luminosity sources, LINERs occupy the lower left-hand corner of the Group 2 AGN dispersion in
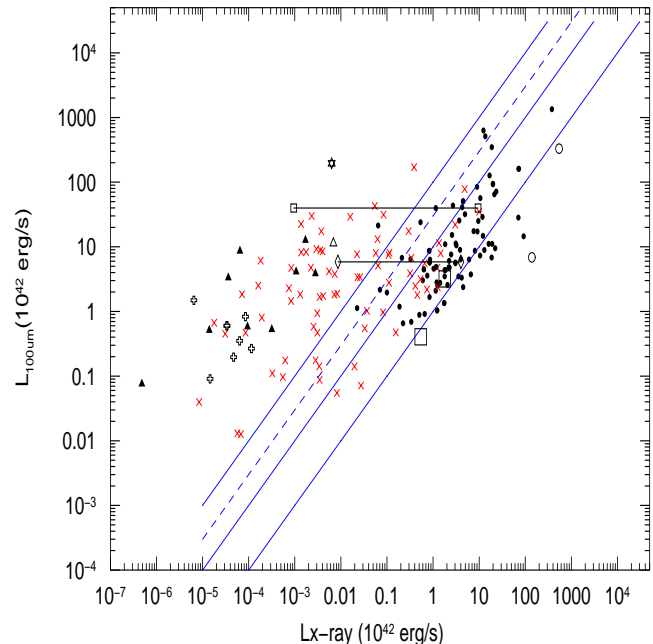

Figure 4. As Fig. 3 except we plot mean 100μm IR luminosity (from IRAS) against mean observed 2-10keV X-ray luminosity for our AGN sample. Also highlighted are the non-Seyfert AGN in our sample. Open crosses in the lower left-hand corner are LINERs and filled-in triangles denote LINERs plus H_{II} regions.

Fig. 4. The LINERs with associated H_{II} regions have generally higher IR luminosities than the 'pure' LINERs, but the X-ray luminosities remain fairly low.

Figures 3 and 4 both show a very clear distinction between the observed luminosity ratios (and their dispersions) for group 1 and group 2 AGN. However, based on the modelled intrinsic 2-10keV X-ray luminosity, Krabbe et al. (2001); Horst et al. (2007) found that the near-IR to X-ray luminosity ratios for group 1 and group 2 AGN were very similar. Figure 5 is as Fig. 3, but with open circles denoting AGN from the study by Horst et al. (2007) and the ranges of *intrinsic* luminosity ratio established by Horst et al. (2007) for group 1 (solid lines) and group 2 (dashed lines) AGN. The dispersion in the luminosity ratio of our group 1 AGN matches that found by Horst et al. (2007) quite well, indicating that observed and intrinsic 2-10keV X-ray luminosities are similar in most group 1 AGN. Our group 2 population seems to diverge dramatically in luminosity ratio from the range found by Horst et al. (2007), suggesting that the observed and intrinsic 2-10keV luminosities in group 2 AGN are indeed dramatically different. However, Horst et al. (2007) estimate the intrinsic X-ray luminosity in the group 2 AGN based on different model fits in the literature, which (a) can vary for the same AGN dataset and which (b) lead to model-dependent constraints on AGN structure (e.g. a clumpy torus as suggested by Horst et al. (2007)). By contrast, an IR-X-ray luminosity ratio based on the observed 2-10keV X-ray luminosity (as in Fig. 5) will help us avoid model assumptions about AGN structure and the AGN environment (see §6 below).

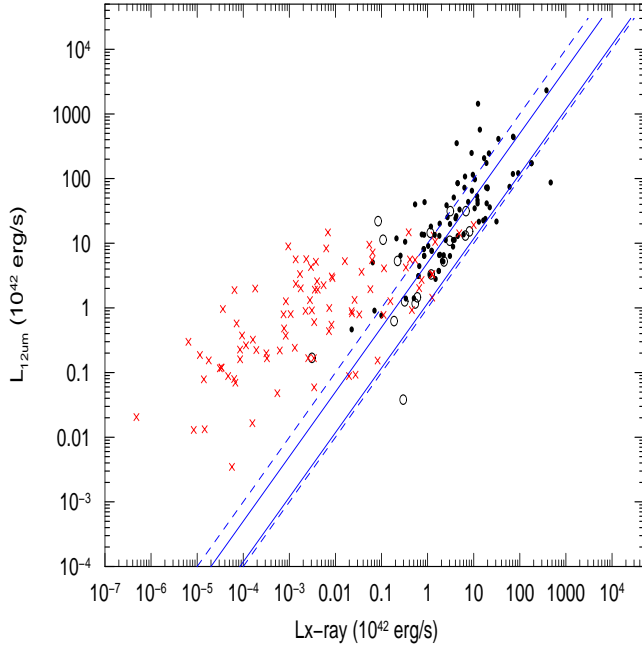The observed IR band emission from AGN should consist of some fraction of reprocessed radiation

Figure 5. As for Fig. 2, except open circles are AGN from the survey of Horst et al. (2007). Solid lines indicate the range of luminosity ratio found by Horst et al. (2007) for group 1 AGN, based on modelled intrinsic 2-10keV X-ray luminosity. Dashed lines indicate the range of luminosity ratio found by Horst et al. (2007) for group 2 AGN based on modelled intrinsic 2-10keV X-ray luminosity.
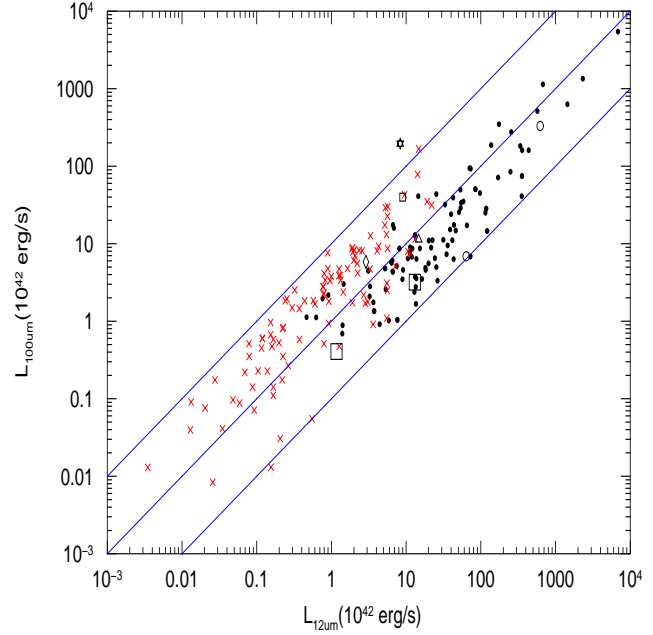

Figure 6. Mean 12μm IR luminosity (from IRAS) plotted against mean 100μm IR luminosity for the AGN in our sample. Symbols & colours are as in Fig. 3. Also plotted are lines of constant luminosity ratio ($L_{100\mu m}/L_{12\mu m}$=10,1,0.1).

(NGC 4945- open square), Circinus (open diamond) and NGC 1068 (open triangle) respectively.

from the AGN typically peaking in the mid-IR (e.g. Efstathiou et al. (2000)) and some fraction of emission from star formation typically peaking in the far-IR (e.g. Efstathiou & Rowan-Robinson (1995); Sirocky et al. (2008); Mas-Hesse et al. (2008)) plus intrinsic IR from the SED. Therefore, by comparing the observed mid- and far-IR luminosities in group 1 and group 2 AGN, we may be able to distinguish dominant components of IR in different AGN.

Figure 6 shows the mean far-IR (100μm) luminosity plotted against the mean mid-IR (12μm) luminosity for the 225 AGN in our sample without jets, for which both mid-IR and far-IR data were available. 115 AGN are group 1 (black circles), 110 are group 2 (red crosses). Also plotted are lines denoting constant luminosity ratios of $10, 1, 0.1$ respectively. The populations of group 1 and group 2 AGN are very well separated by the luminosity ratio $L_{100\mu m}/L_{12\mu m} = 1$. Only 22/110 ($\sim 20\%$) of group 2 have $L_{100\mu m}/L_{12\mu m} < 1$. The three outlier group 2 AGN in this plot near the $L_{100\mu m}/L_{12\mu m} = 0.1$ line are nearby LINERs that could be cross-classified. From Fig. 6 we can say that the $L_{100\mu m}/L_{12\mu m}$ ratios for group 2 AGN are on average an order of magnitude larger than those for group 1 AGN. The dispersion in both groups is also similar (roughly an order of magnitude). The $L_{100\mu m}/L_{12\mu m}$ ratio also appears to neatly separate out the 'archetypal' Group 2 AGN, in order of most 'cold' (100μm) dust to least 'cold' dust. Evidently the starburst Arp 220 (open star) has by far the highest value of $L_{100\mu m}/L_{12\mu m}$ (as we should expect e.g. Efstathiou et al. (2000); Mas-Hesse et al. (2008)) followed by the Compton-thick AGN seen in transmission

5 RULING OUT SELECTION BIAS

Fig. 3 demonstrates that the luminosity ratio ($R_{ir/x}$) of the 245 AGN in our sample is not a scatterplot. So, are the unoccupied regions of the $R_{ir/x}$ plot genuinely depopulated, providing a model-independent constraint on AGN structure, or is there a selection effect at work? First, flux limits from all-sky surveys in both the IR band and the X-ray band allow us to establish which regions of $R_{ir/x}$ are probably genuinely unoccupied by AGN. Fig. 7 is as Fig. 3 except superimposed are flux detectability thresholds from (solid line) the ROSAT All-sky survey (2×10^{-13} ergs cm^{-2}s^{-1} from Voges (1993)) and the IRAS 12μm complete sample (~ 0.3Jy from Sanders et al. (2003)), corresponding to luminosity distances of 10Mpc,100Mpc and 1000Mpc. The ROSAT survey was carried out in soft X-rays (0.1-2.4keV) and will undercount heavily absorbed AGN (ie Group 2 AGN) in this band. So, since Group 1 AGN are not very heavily absorbed in the soft X-ray band and since 115/116 of the Group 1 AGN in our sample are detectable in the 2-10keV band at ROSAT flux levels, the ROSAT limits are a reasonable proxy for X-ray flux limits for Group 1 AGN. This is the best that we can do since surveys overlapping the 2-10keV band, are neither all-sky nor complete (Revnitsev et al. 2004; Tueller et al. 2008). Distances of a few tens of Mpc correspond to a volume of space spanning all varieties of nuclear activity, so it seems probable that empty regions in the upper right corner of $R_{ir/x}$ are genuinely depopulated by luminous (Group 1) AGN. Any Group 1 AGN undiscovered in the X-ray band, must lie to the left of their corresponding vertical luminos-
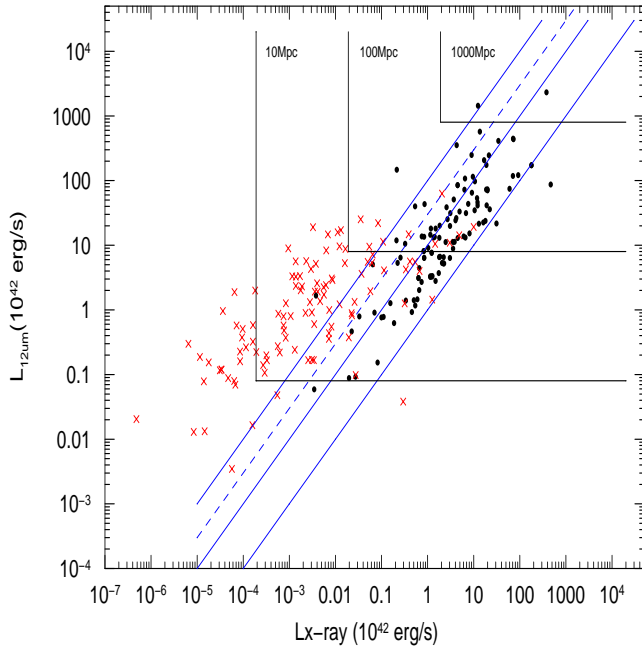
Figure 7. As Fig. 3, except also indicated are the luminosity lower limits from the IRAS 12µm survey (0.3Jy, from Sanders et al. (2003)) and the ROSAT All-Sky survey (2×10^{-13} ergs cm^{-2}s^{-1} from Voges (1993)). The ROSAT limits are from soft (0.1-2.4keV) X-rays and are therefore a reasonable proxy flux limit for AGN unlikely to be very heavily absorbed in the soft X-ray band (our Group 1 AGN). The IRAS flux limits apply to both Group 1 and Group 2 AGN. AGN at <10Mpc,<100Mpc and <1000Mpc distances that have not been detected must lie in the region of parameter space to the left of the appropriate X-ray limit (Group 1 AGN only) and below the appropriate indicated IR limit (both Group 1 and Group 2 AGN).

ity distance detection limit (e.g. a Type 1 QSO at 100Mpc undiscovered in X-rays, must lie to the left of the vertical 100Mpc line). Similarly, any low luminosity AGN, undiscovered at 12µm must lie below the corresponding horizontal luminosity distance detection limit (e.g. a Type 2 QSO at 100Mpc undiscovered at 12µm must lie below the horizontal 100Mpc line).

Second, we also need to check that the dispersion of AGN is not unduly affected by picking up higher luminosity AGN at relatively higher redshifts. In Fig. 8 we plot the 109 AGN (56 Group 1 and 53 Group 2 AGN) in the redshift range $z = [0.005, 0.05]$ (or ~[20,200]Mpc). Fig. 8 excludes the highest and lowest luminosity AGN from both Groups. From Fig. 8, 53/56 Group 1 AGN have $1 < R_{ir/x} < 30$, a similar ratio to the 103/115 Group 1 AGN in the same range, using our full sample. The Spearman rank correlation coefficient (S_{rc}) for our complete Group 1 distribution (without jets) is 0.69 with a strong statistial significance (5×10^{-8}). When we split our Group 1 distribution into those AGN at $z < 0.05$ (65/112) and $z > 0.05$ (47/112), we find that S_{rc} is statistically significant at 0.71 and 0.67 respectively. We also find that the mean value of $R_{ir/x}$ for both these $z < 0.05$ and $z > 0.05$ Group 1 AGN populations are consistent with each other and with the mean value of $R_{ir/x}$ of the complete Group 1 population, within the mean absolute deviation of each population. Furthermore, the T-statistic for these 'low' and 'high' z Group 1 AGN has a significance
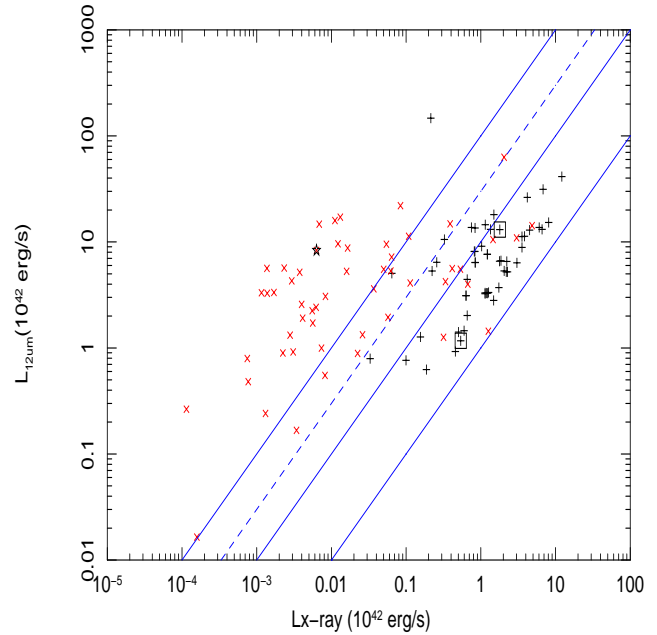

Figure 8. As Fig. 3, except we only plot those AGN in the redshift range z=[0.005,0.05] (or ~[20,200]Mpc). For clarity, we denote the Group 1 AGN with plus symbols. Note that 53/56 Group 1 AGN lie in the range $30 < R_{ir/x} < 1$, a similar ratio to the 103/115 Group 1 AGN in Fig. 3.

of 0.5, indicating that the $z < 0.05$ and $z > 0.05$ populations do not originate in distributions with substantially different mean values of $R_{ir/x}$. In future work, we anticipate extending our sample with a view to obtaining strong statistical constraints on the value of $R_{ir/x}$ in AGN.

Another way of assessing the depopulation of regions of the $R_{ir/x}$ plot is by considering the dispersion of complete samples of AGN. The samples of Rush et al. (1993) and Sanders et al. (2003) in Table 1 correspond to complete, flux-limited IRAS samples at 12µm and 60µm respectively. However, in each case, only ~ 15% of each sample have 2-10keV X-ray data. However, the sample of Rush et al. (1993) in particular spans most of our range of L_x, L_{12um} space, so a comparison of our sample with Rush et al. (1993) could tell us if we are under-sampling a particular region of parameter space. Fig. 9 is as Fig. 2, except that only AGN from Rush et al. (1993) are plotted.

Clearly, the subset of the complete 12µm IRAS AGN sample span the full range of $R_{ir/x}$ for Group 2 AGN and most of the range of $R_{ir/x}$ for Group 1 AGN. Furthermore, the 12µm sample subset does not stake out otherwise unoccupied regions of $R_{ir/x}$ space. It is possible that the remainder of the complete IRAS samples picked out AGN that live in e.g. the top-left of Fig. 2, i.e. low L_x and large L_{ir}. However, an additional ~ 20% IRAS AGN had 0.2−4.0keV *Einstein* X-ray flux measurements, yielding similar values of $R_{ir/x}$ to those in Fig. 9 (see also Green, Anderson & Ward (1992) and Boller et al. (1992)). The sample of AGN studied by Tueller et al. (2008) is not limited by X-ray absorption, so it is useful to consider the range of $R_{ir/x}$ spanned by these AGN. Fig. 10 is as Fig. 2, but indicates those AGN from Tueller et al. (2008). Once again, it is clear that this
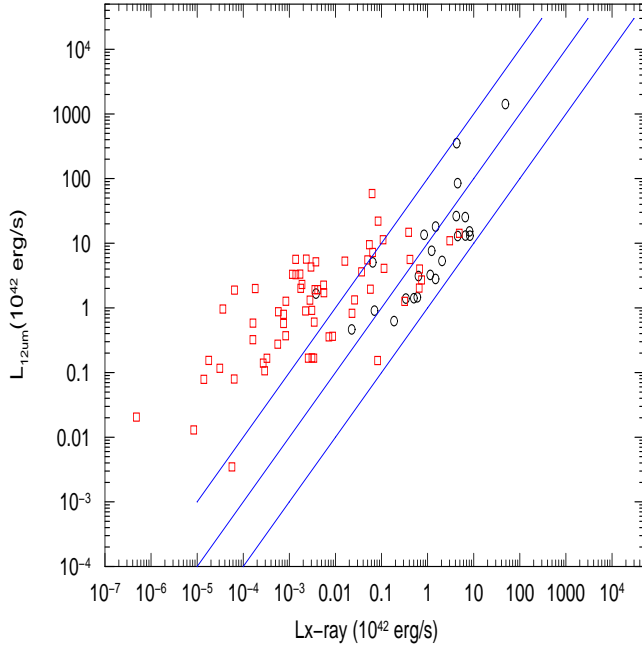
Figure 9. As Fig. 2, except we only plot those AGN from the complete 12μm IRAS flux-limited sample Rush et al. (1993) with 2-10keV X-ray data. Open red squares denote Group 2 AGN and open black circles denote Group 1 AGN from Rush et al. (1993).
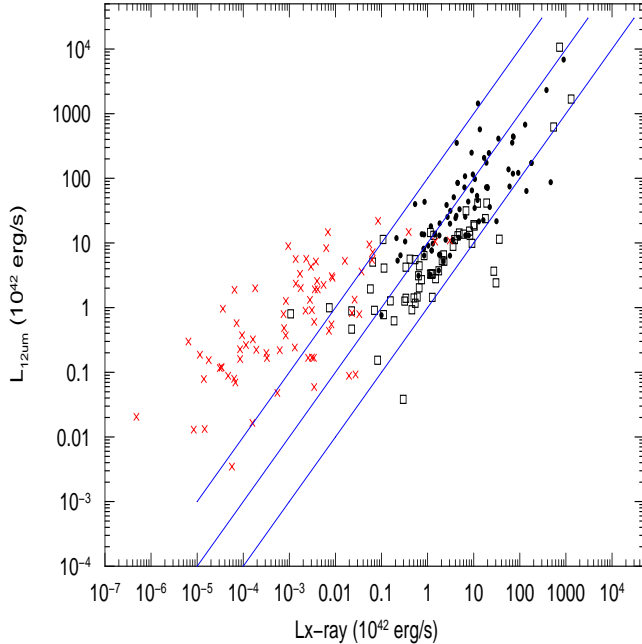

Figure 11. As Fig. 3, except we plot filled-in circles a new sample of 150 AGN from the deep surveys of Miyaji et al. (2004); Polletta et al. (2006); Tajer et al. (2007). The observed luminosity ratio for these deep ($z \sim 1$) AGN uses 2-10keV observed fluxes which correspond to $\sim 4 - 20$keV in the AGN restframe. Therefore the luminosity ratio $R_{ir/x}$ will be a factor of a few higher (ie. displaced slightly leftwards on the plot) on average than the Group 1 AGN in Fig. 3.

the deep surveys (typically z∼ 1), an observed IR luminosity at 24μm corresponds *approximately* to an AGN-frame 12μm IR luminosity (see e.g. Treister, Krolik & Dullemond (2008)) and a 2-10 keV X-ray luminosity corresponds to an AGN-frame $4-20$ keV X-ray luminosity (which will typically lie within a factor of a few of the actual 2-10keV luminosity), so luminosity ratios $R_{ir/x}$ for these deep AGN will systematically be a factor of a few higher on average than for the local AGN in Fig. 3.

From Fig. 11, even without considering the systematic overestimate of $R_{ir/x}$ above, the high z AGN appear to closely follow the luminosity ratio for the Group 1 AGN in Fig. 3 and very few lie in the Group 2 AGN region (8/150 have $R_{ir/x} > 100$) or in the blank areas of our luminosity plot. While there are clearly many caveats to using such deep survey data (not least assumptions about the AGN SED shape based on the IR spectrum), it is intriguing that, even with our very simple approach, the deep survey points should follow very closely the low-z Group 1 AGN dispersion and not fill blank regions of the luminosity ratio plots. It is also comforting that our main distribution of Group 1 AGN in Fig. 3 is also consistent with the dispersion of the population of AGN in Mushotzky et al. (2008), which, since the X-rays are 14-195keV, should be independent of X-ray absorption.

Figure 10. As Fig. 2, except also indicated as open circles are those AGN in the BAT X-ray sample Tueller et al. (2008), which is unlimited by X-ray absorption.

sample spans the existing ranges of $R_{ir/x}$ space and does not stake out otherwise unoccupied regions.

In order to test the effect of AGN redshift on our sample, we studied an independent sample of 150 additional high-z AGN observed from deep surveys with XMM-Newton and Chandra (Miyaji et al. 2004; Polletta et al. 2006; Tajer et al. 2007). At the high redshifts of AGN in
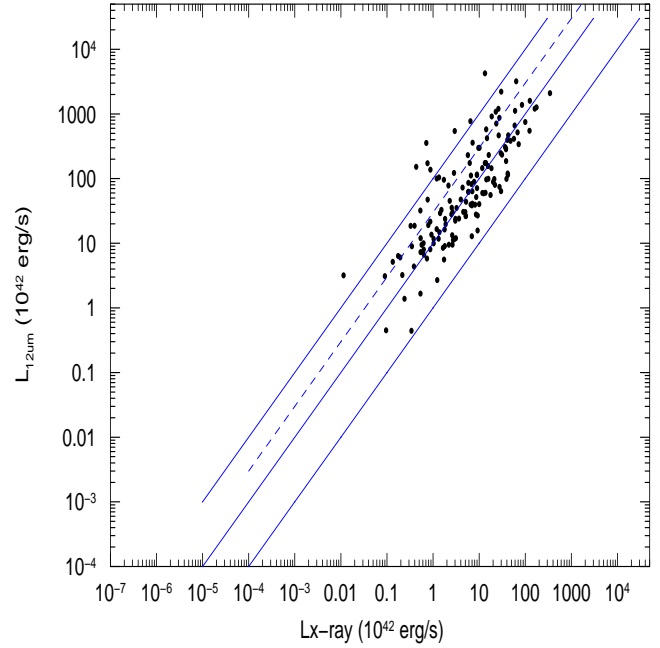
6 DISCUSSION

Much of the IR emission from active galactic nuclei should come from reprocessed X-ray emission. There should also be

some component of intrinsic IR emission in the SED (including non-thermal IR; although we shall ignore the complication of jets in the following discussion) and any remaining nuclear IR emission should be due to star formation in the thick dust in the nucleus. Whether the dust lives in a torus (doughnut) or in clumps, we can characterize the IR emission from 'active' nuclei (without prominent jets) as:

$$
\begin{aligned}
L_{IR} &= L_{AGN} + L_{stars} \\
&= L_x g_{unit} \left[g_{sed} + \left(\tfrac{\Omega}{4\pi} \right) f_{abs} g_{repro} f_{Lbol} \right] + L_{stars}
\end{aligned} \quad (1)
$$

where g_{unit} is a numerical factor from converting L_x, the 2-10keV intrinsic X-ray luminosity to the same units as L_{IR}, g_{sed} is a factor corresponding to intrinsic IR emitted by the AGN (normalized to L_x), $\Omega/4\pi$ is the covering factor of the reprocessing material, f_{abs} is the fraction of the 2-10keV radiation absorbed, g_{repro} is a factor depending on the details of the reprocessing physics (including dust size & chemistry), f_{Lbol} is the fraction of the bolometric luminosity absorbed by the cool dust.

For most group 1 AGN we expect, $L_{AGN} \gg L_{stars}$, so the observed luminosity ratio for most group 1 AGN should be

$$
\frac{L_{IR}}{L_x} \approx R_{i/o} g_{unit} [g_{sed} + \left(\frac{\Omega}{4\pi} \right) f_{abs} g_{repro} f_{Lbol}] \quad (2)
$$

where $R_{i/o}$ is the ratio of intrinsic to observed 2-10keV X-ray luminosity and is a function of the column of X-ray absorbing material along the observers' sightline. From Figs. 3 and 4, the dispersion in $R_{ir/x}$ for most ($\sim 90\%$) group 1 AGN is a factor of 30 or less. Therefore the total combined variation in all the multipliers in equation 2 must be less than thirty for most Group 1 AGN. The factor f_{abs} is a function both of the covering fraction of the reprocessing material and its column density ($f_{abs} = f_c f_{Nh}$). Using XSPEC, we tested the effect of column density on f_{abs} by investigating the change in X-ray energy for absorbing column density in the range $N_H = [10^{19}, 10^{24}] \text{cm}^{-2}$. We found that a factor of 10^5 increase in absorbing column density, only produced a factor of five in the X-ray energy absorbed (similar to the results of Pier & Krolik (1993) and Efstathiou et al. (2000)). So a 'naked' Group 1 AGN without substantial amounts of absorbing material (e.g. a torus) in its environment, should have an IR flux only $\sim 1/5$th that of a Group 1 AGN surrounded by substantial amounts of dust (not necessarily in the sightline). Therefore, a *total* dispersion of $1 < R_{ir/x} < 30$ for most Group 1 AGN, will include a factor of $\leqslant 5$ for f_{Nh}, indicating that $f_{unit}, g_{sed}, g_{repro}, f_{Lbol}, f_c$ could vary collectively by as little as a factor of six, across all Group 1 AGN. Thus, the covering factor and fraction of absorbing material (clouds, torus, flared disk etc), the composition of the material (dust chemistry, abundance, size), the column density of the material and the SED X-ray to IR ratio in group 1 AGN *collectively* vary by a factor of thirty or less and possibly by as little as a factor of six. Note that this is a *model-independent result*. We have not assumed that the absorbers must either be in a torus or clouds or some combination. Such a tight dispersion among Group 1 AGN severely restricts models of accretion, geometry and physical conditions in AGN. These Group 1 AGN collectively span a range of $\sim 10^3$ in central black hole mass (e.g. Peterson et al. (2004)), suggesting that independent of jets, the central engines of Group 1 AGN are quite *remarkably*

similar. Again, it is worth noting that this remarkably small variation in AGN properties is based on *observed* quantities and is therefore model-independent.

Group 2 AGN, with associated star-forming regions, could have $L_{AGN} < L_{stars}$ in equation 1. Furthermore, Fig. 6 indicates that the ratio of cold dust to warm dust (indicative of star formation) is an order of magnitude larger in group 2 AGN than in group 1 AGN. The fact that dispersion in $R_{ir/x}$ is 2-3 orders of magnitude larger for Group 2 AGN than for Group 1 AGN, indicates either that (a) observed $L_x \ll$ intrinsic L_x or that (b) $L_{stars} \gg L_{AGN}$ in Group 2 AGN or both. Mushotzky et al. (2008) find that the intrinsic X-ray luminosity for Group 2 AGN is comparable to that for Group 1 AGN, so in most cases observed L_x is probably substantially lower than intrinsic L_x. It is also possible that L_{stars} is intrinsically greater in group 2 AGN than in group 1 AGN.

7   CONCLUSIONS

Our aim was to compare common observed AGN properties that encompass the continuum of AGN activity in an effort to, if possible, derive model-independent constraints on AGN structure and the accretion neighbourhood. We studied the observed X-ray to IR luminosity ratios of a heterogeneous sample of 245 galaxies from the literature and, in spite of our simple approach, AGN variability and non-simultaneity of most of the data, we found strong trends.

Fig. 3 reveals the emergence of observed 'activity' at $L_{IR}, L_X > 10^{42} \text{ergs}^{-1}$. Below these luminosities, AGN may compete with X-ray and IR emitters in the host galaxy (such as ULXs, see e.g. Miniutti et al. (2006)) or may be obscured by large columns of absorbing material. Since emission from jets considerably complicates our interpretation of the observed luminosity ratios, we only considered those AGN without prominent observed jets. We find that AGN considered 'face-on' or unobscured in the standard model (our group 1) are tightly clustered by observed luminosity ratio ($\sim 90\%$ have $1 < R_{ir/x} < 30$), indicating that there is very little variation between individual group 1 AGN in: (a) intrinsic SED (i.e. accretion flow, whether ADAF, tubulent disk or both), (b) solid angle of the reprocessing ($X \rightarrow IR$) absorber (whether clouds, torus, flared-disk or some combination) and (c) details of the absorbing material (chemistry & dust grain sizes). Thus, Fig. 3 demonstrates that underlying Group 1 AGN is a remarkably uniform phenomenon.

Fig. 3 shows a clear difference in $R_{ir/x}$ between unobscured AGN (group 1) and obscured & low luminosity AGN (our group 2). Despite the fact that our sample is *not* complete, our findings for the dispersion of AGN are confirmed in a comparison with other, independent AGN samples (e.g. Tueller et al. (2008); Mushotzky et al. (2008), which are not limited by X-ray absorption, or Tajer et al. (2007); Polletta et al. (2006); Miyaji et al. (2004) from $z \sim 1$). Furthermore, subsets of our sample of 245 AGN are derived from complete IRAS samples (Sanders et al. 2003; Rush et al. 1993) and these subsets at least do not span values of $R_{ir/x}$ different from the rest of our sample. Bias is of course a potential problem with any approach such as ours, but it is comforting that we can find some independent verification for our simple, model-independent approach. Es-

timates of the intrinsic 2-10 keV luminosity for Compton-thick AGN from very hard X-ray (absorption independent) observations (e.g. Tueller et al. (2008); Matt et al. (1999); Itoh et al. (2008)) reveal that the intrinsic luminosity ratio is consistent with the group 1 AGN (in agreement with the findings of e.g. Lutz et al. (2001); Krabbe et al. (2001); Horst et al. (2007); Mushotzky et al. (2008)). However, unlike Lutz et al. (2001); Krabbe et al. (2001); Horst et al. (2007) we have endeavoured to avoid the highly model-dependent business of estimating intrinsic 2-10keV X-ray luminosity of group 2 AGN based on the 2-10keV observed luminosity. We also studied the far-IR to mid-IR luminosity ratios of the nuclei in our sample. We found that the 100μm to 12μm luminosity ratio ($L_{100\mu m}/L_{12\mu m} \sim 1$) is an extremely effective separator of the group 1(unobscured) and group 2 (obscured & low luminosity) populations (see Fig.6). Using archetypal AGN as a guide, this plot ranks group 2 AGN in order of decreasing luminosity ratio for increasing obscuration.

In principle our approach could be applied to intermediate mass black holes (IMBHs) and Galactic black hole candidates (GBHCs) to investigate the accretion neighbourhood around black holes on all mass scales. The outstanding question is whether reprocessing material around IMBHs and GBHCs is substantially different in covering factor, structure, chemistry or reprocessing details from that around AGN. Are a flared disk or dusty torus associated with a minimum mass scale, or are we looking at a basically identical phenomenon across 7-8 orders of magnitude in mass?

ACKNOWLEDGEMENTS

REFERENCES

Antonucci R. R. J., 1993, ARA&A, 31, 473

Bian W. & Zhao Y., 2003, MNRAS, 343, 164

Boller Th., Meurs E.J.A., Brinkmann W., Fink H., Zimmermann U. & Adorf H.-M., 1992, A&A, 261, 57

Bonatto C., Pastoriza M.G., Alloin D. & Bica E., 1998, A&A, 334, 439

Boroson T.A. & Green R.F., ApJS, 80, 109

Botte V., Ciroi S., diMille F., Rafanelli P. & Romano A., 2005, MNRAS, 356, 789

Buchanan C.L., Gallimore J.F., O'Dea C.P., Baum S.A., Axon D.J., Robinson A., Elitzur M. & Elvis M., 2006, ApJ, 132, 401

Efstathiou A. & Rowan-Robinson M., 1995, MNRAS, 273, 649

Efstathiou A., Rowan-Robinson M. & Siebenmorgen R., 2000, MNRAS, 313, 734

Eracleous M. & Halpern J.P., 1994, ApJS, 90, 1

Foschini L. *et al.* 2006, A&A, 453, 829

Gonzalez Delgado R. M., Perez E., Tadhunter C., Vilchez J.M. & Rodriquez-Espinoza J.M., 1997, ApJS, 108, 155

Green P. J., Anderson S.F. & Ward M.J., 1992, MNRAS, 254, 30

Grupe D., Beuermann K., Mannheim K. & Thomas H.-C., 1999, A&A, 350, 805

Ho L., Fillippenko A.V. & Sargent W.L.W., 1997, ApJ, 487, 568

Horst H., Ghandi P., Smette A. & Duschl W.J., 2007, A&A (accepted), astro-ph/0711.3734

Itoh T. *et al.* 2008, PASJ, 60, 251

Krabbe A., Böker T. & Maiolino R., 2001, ApJ, 557, 626

Kraft R. P. *et al.* 2000, ApJ, 531, 9

Kukula M. J., Dunlop J.S., Hughes D.H. & Rawlings S., 1998, MNRAS, 297, 366

Leighly K., 1999, ApJS, 125, 317

Lutz D., Maiolino R., Spoon H. W. W. & Moorwood A. F. M. 2004, A&A, 418, 465

Malizia A., Bassani L., Zhang S.N., Dean A.J., Paciesas W.S. & Palumbo G.G.C., 1999, ApJ, 519, 637

Markowitz A. & Edelson R., 1999, ApJ, 617, 939

Matt G. *et al.* 1999, A&A, 341, L39

Mas-Hesse J.M., Oti-Floranes H. & Cervino M., 2008, A&A, 483, 71

McKernan B. & Yaqoob T., 1998, ApJ, 501, L29

McKernan B., Yaqoob T. & Reynolds C. S., 2007, MNRAS, 379, 1359

Miller P., Rawlings S. & Saunders R., 1993, MNRAS, 263, 425

Miller L., Turner T.J. & Reeves J.N., 2008, MNRAS, 483, 437

Miniutti G. *et al.* 2006, MNRAS, 373, L1

Miyaji T., Sarajedini V., Griffiths R.E., Yamada T., Schurch M., Cristobal-Hornillos D. & Motohara K., 2004, AJ, 127, 3180

Mushotzky R. F., Winter L.M., McIntosh D.H. & Tueller J., 2008, ApJL (accepted), astro-ph/0807.4695

Nagar N. M., Falcke H., Wilson A.S., 2005, A&A, 435, 521

Pier E. A. & Krolik J. H., 1993, ApJ, 418, 673

Perola G.C., Matt G., Cappi M., Fiore F., Guainazzi M., Maraschi L., Petrucci P.O. & Piro L., 2002, A&A, 389, 802

Peterson B. M. *et al.* 2004, ApJ, 613, 682

Polletta M. del C. *et al.* 2006, ApJ, 642, 673

Porquet D., Reeves J.N., Markowitz A., Turner T.J., Miller L. & Nandra K., 2007, A&A, 466, 23

Revnivtsev M., Sazonov S., Jahoda, K. & Gilfanov M., 2004, A&A, 418, 927

Risaliti G., Elvis M. & Nicastro F., 2002, ApJ, 571, 234

Rush B., Malkan M.A. & Spinoglio L., 1993, ApJS, 89, 1

Sanders D.B., Mazzarella J.M., Kim D.C., Surace J.A. & Soifer B.T., 2003, AJ, 126, 1607

Schade D.J., Boyle B.J. & Letawsky M., 2000, MNRAS, 315, 498

Shinozaki K., Miyaji T., Ishisaki Y., Ueda Y. & Ogasaka Y., 2006, AJ, 131, 2843

Sirocky M. M., Levenson N. A., Elitzur M., Spoon H. W. W. & Armus L., 2008, ApJ, 678, 729

Smith D.A. & Done C., 1996, MNRAS, 280, 355

Spergel D.N. *et al.* 2003, ApJS, 148, 175

Tajer M. et al., 2007, A&A, 467, 73

Treister E., Krolik J. H. & Dullemond C., 2008, ApJ, 679, 140

Tueller J., Mushotzky R.F., Barthelmy S., Cannizzo J.K., Gehrels N., Markwardt C.B., Skinner G.K. & Winter L. M., 2008, ApJ, 681, XXX (astro-ph/0711.4130)

Turner T. J., George I.M., Nandra K. & Turcan D., 1999, ApJ, 524, 667

Veilleux S.B. & Osterbrock D.E., 1987, ApJS, 63, 295

Voges W., 1993, AdSpR, 13, 391

Winter L. M., Mushotzky R.F., Tueller J. & Markwardt C., 2008, ApJ, 674, 686